3.3 Verification of the model

3.3.1 The conical island experiment

The 1+1 computations (one horizontal and one vertical directions) described in chapter 2 validated different aspects of the numerical performance of the finite-difference scheme (2.7). The 1+1 computations showed that the scheme was robust enough to model not only non-breaking waves but also the runup of weakly nonlinear plunging waves on a plane beach quantitatively and qualitatively correctly. Since exactly the same scheme is used for the 2+1 model by applying the splitting technique, the dispersion and the mass-conservation properties are expected to be the same as for two dimensional computations and we will not discuss this topic here. To test the overall 2+1 algorithm we performed a computer simulation of the conical island experiments described below.

The large scale laboratory experiment of tsunami runup on a circular island was recently conducted at US Army Engineer Waterways Experiment Station (Briggs, Synolakis, Harkins and Green, 1995). The experiment was designed by Synolakis to model the effects of different generation parameters. He used 30m wide and 25m long basin with a conical island near the center to study the runup of a solitary wave on the island. A directional spectral wave generator installed along the wall of the basin produced a plane solitary wave with variable crest length propagating towards the island. Twenty-seven wave gages distributed around the basin recorded free-surface displacement and captured the evolution of the incident solitary wave during its propagation. The runup line was measured at twenty locations around the perimeter of the island after each run. A set of data produced from the ex-

periments is an excellent test for numerical models of long waves and as discussed earlier, it was used as a benchmark problem for the International Long Wave Runup Workshop in Friday Harbor, Washington, 1995.

VTCS-3 was used to simulate some of the conical island experiments. The discretized basin for the numerical computations had a mesh size $\Delta x = \Delta y = 0.15m$ over the flat–bottom part, and $\Delta x = \Delta y = 0.09m$ over the sloping beach of the conical island; the time step $\Delta t = 0.02sec$. The boundary $y = 0$ of the computational domain was the wave generator of the numerical model. The movement of the wave-generator paddles was modeled by inputting the values of the velocity of each paddle every time step. The corresponding boundary condition for the system (3.29) takes the form,

$$p_0^n = u_0 + 2\sqrt{gd_0}, \tag{3.36}$$

where $p_0{}^n = p(0, t+n\Delta t)$ is the boundary value of the Riemann invariant and $u_0{}^n = u(0, t+n\Delta t)$ is the velocity of the paddle movement computed from the paddle trajectory used in the experiment. On the other three boundaries $x = 0$, $x = 30m$ and $y = 25m$, the absorbing boundary conditions (3.32), (3.33) were specified. Moving boundary computations were performed around the conical island shoreline.

Sketch of the basin and the locations of the wave gages are shown on Figure 3.17. Here only a computer simulation of the experiments where the full length of the wave generator was used (4 module symmetric source) is presented. This wave cannot not be considered as an incoming plane wave (a wave with infinitely long crest), since the boundaries

of the basin are absorbing boundaries; therefore the generated wave was a wave with finite crest length of the size of the wave generator.

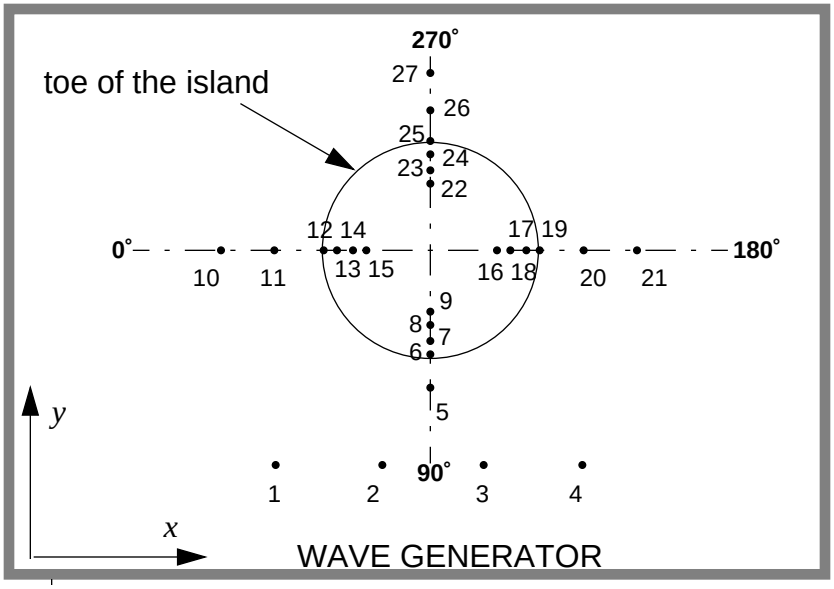

Figure 3.17 Sketch of the basin and location of the wave gages

Figure 3.18 through Figure 3.22 show comparisons among the computed time series and the laboratory wave gage records for the solitary wave with $\eta/d = 0.1$. The figures show that the computed wave simulate well the incident wave and the first reflection from the conical island. The tails of the laboratory record differ from the model predictions, most probably because the boundaries are different. Although, horse-hair absorbers were used on the basin boundaries during the laboratory experiment, reflection from the boundaries was observed during experiment runs. Since the reflection coefficient was not known for this absorber, the radiating or totally absorbing boundary conditions (3.32), (3.33) were used for the computations. These conditions assume no boundaries around the modeled area. Therefore the reflection from the computational boundaries is not present on computed profiles but is evident on the experimental records.

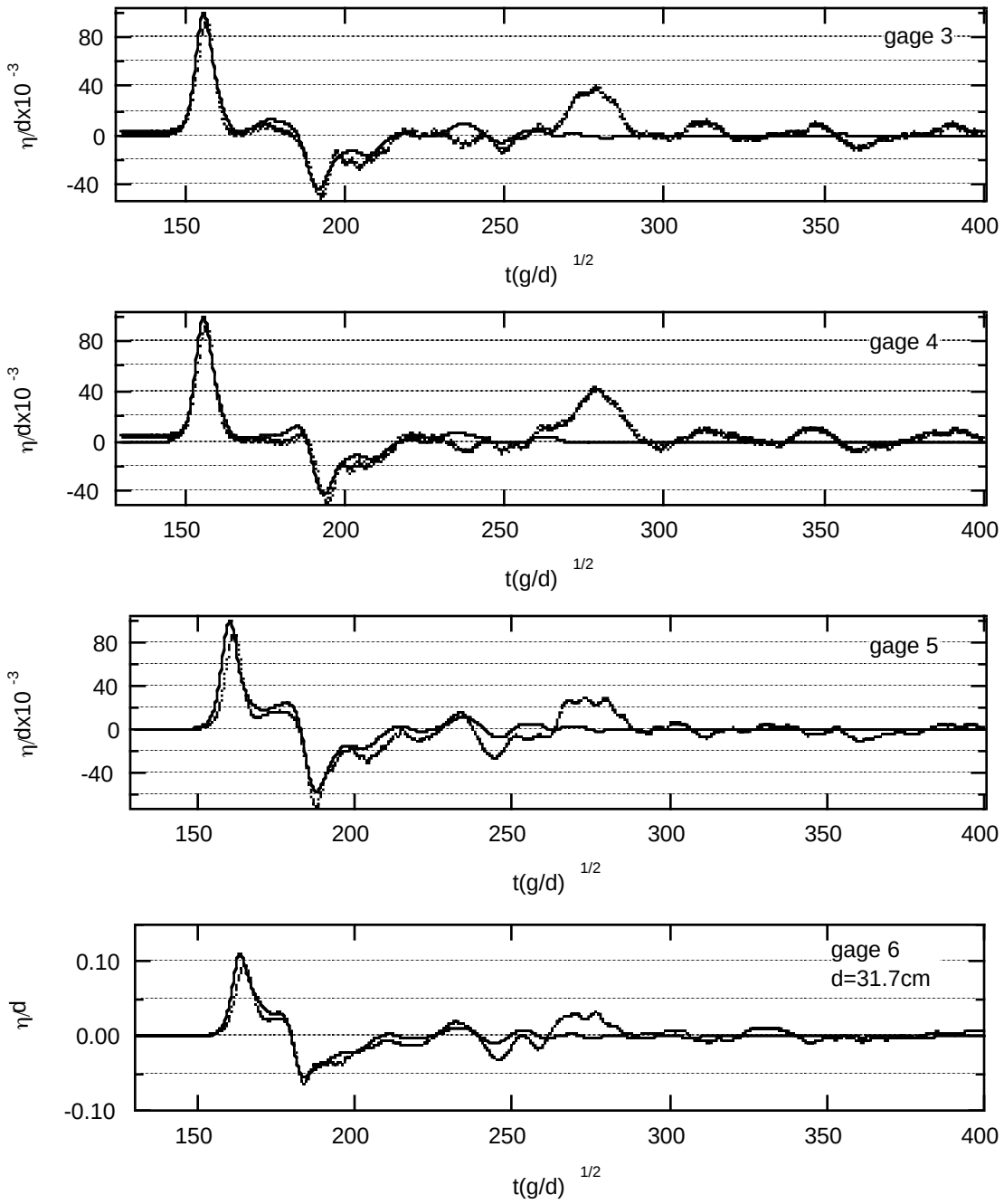

Figure 3.18 Comparison among the computed (solid lines) and laboratory records (dots) for the 0.1 wave.

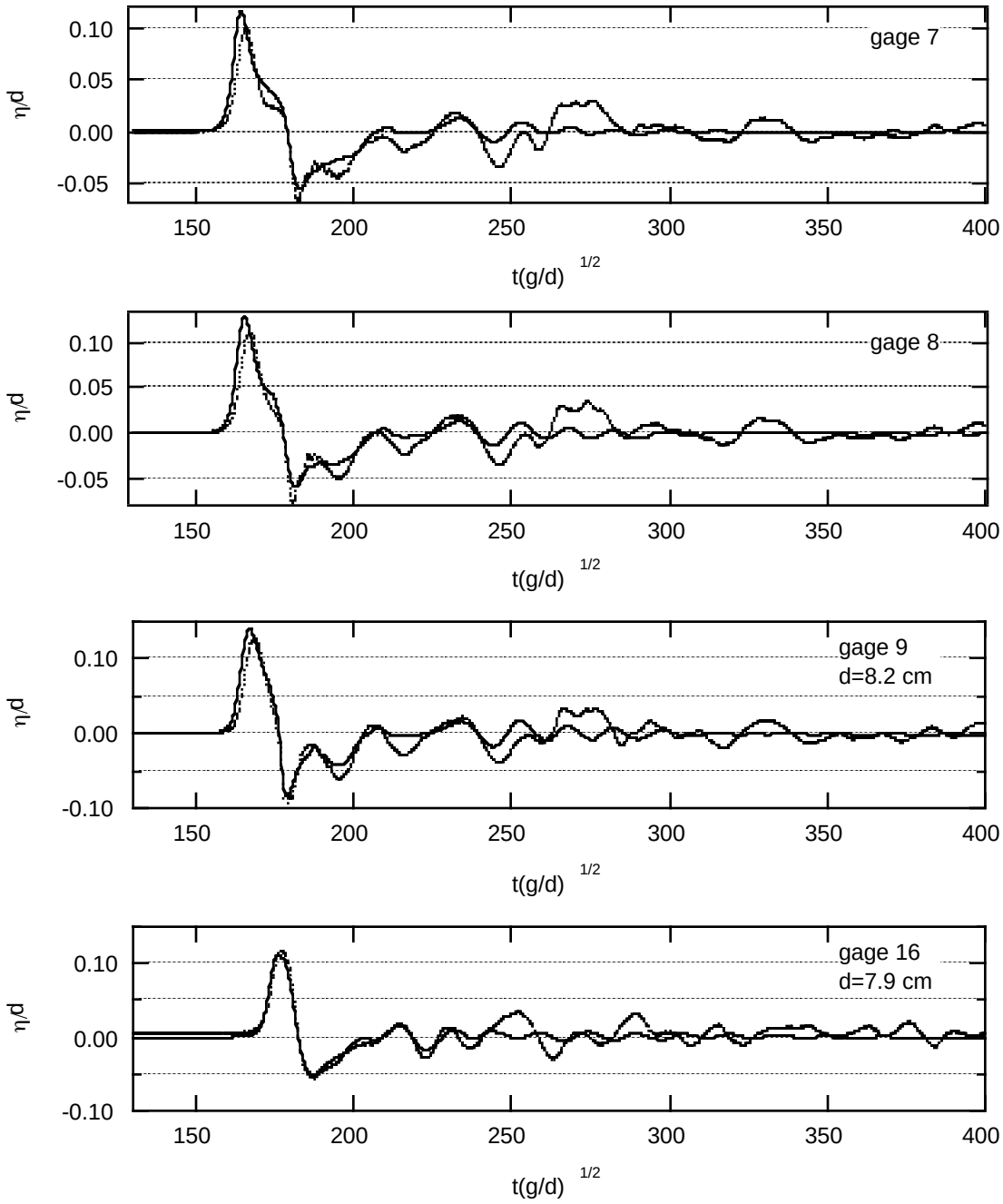

Figure 3.19 Comparison among the computed (solid lines) and laboratory records (dots) for the 0.1 wave.

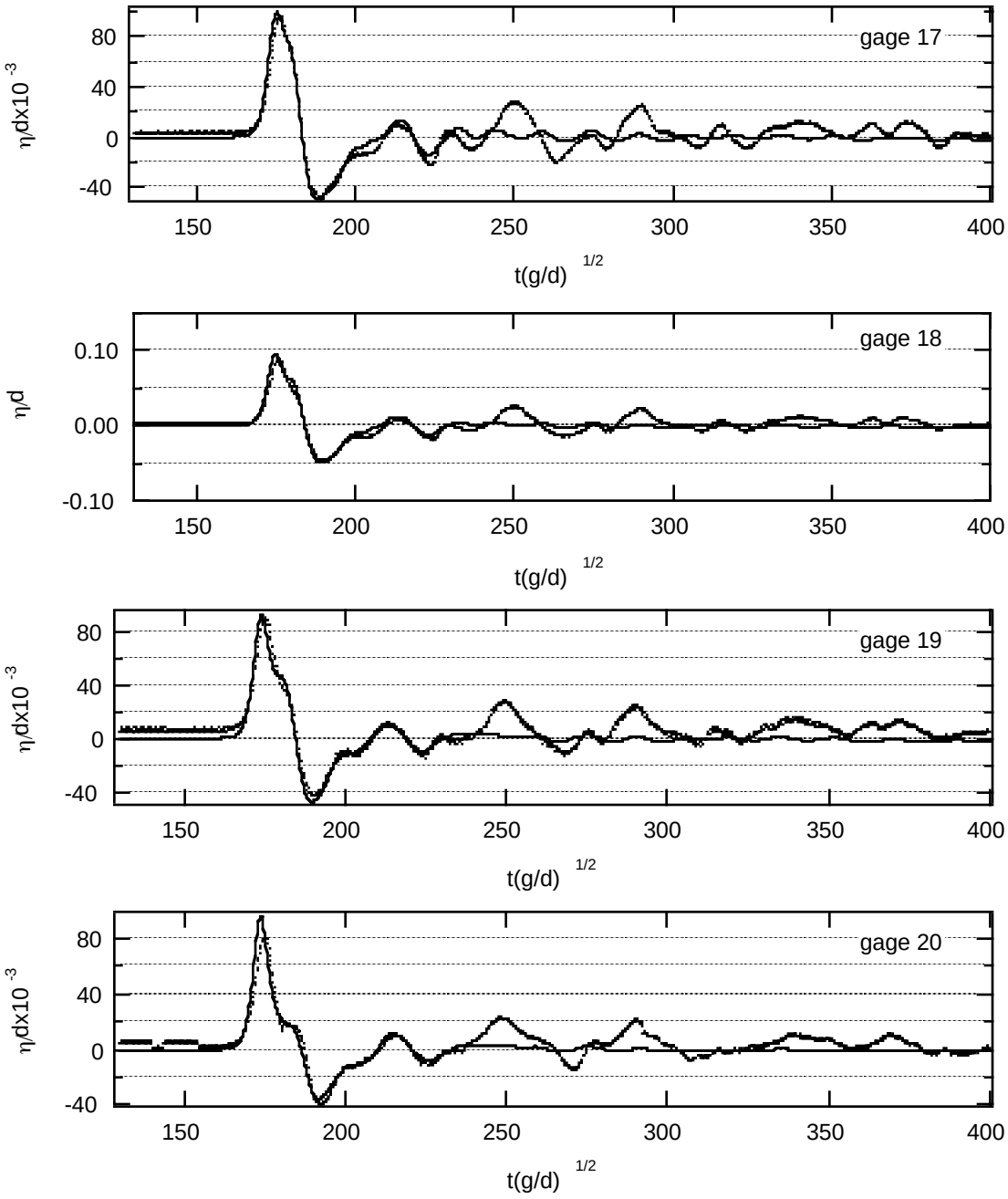

Figure 3.20 Comparison among the computed (solid lines) and laboratory records (dots) for the 0.1 wave.

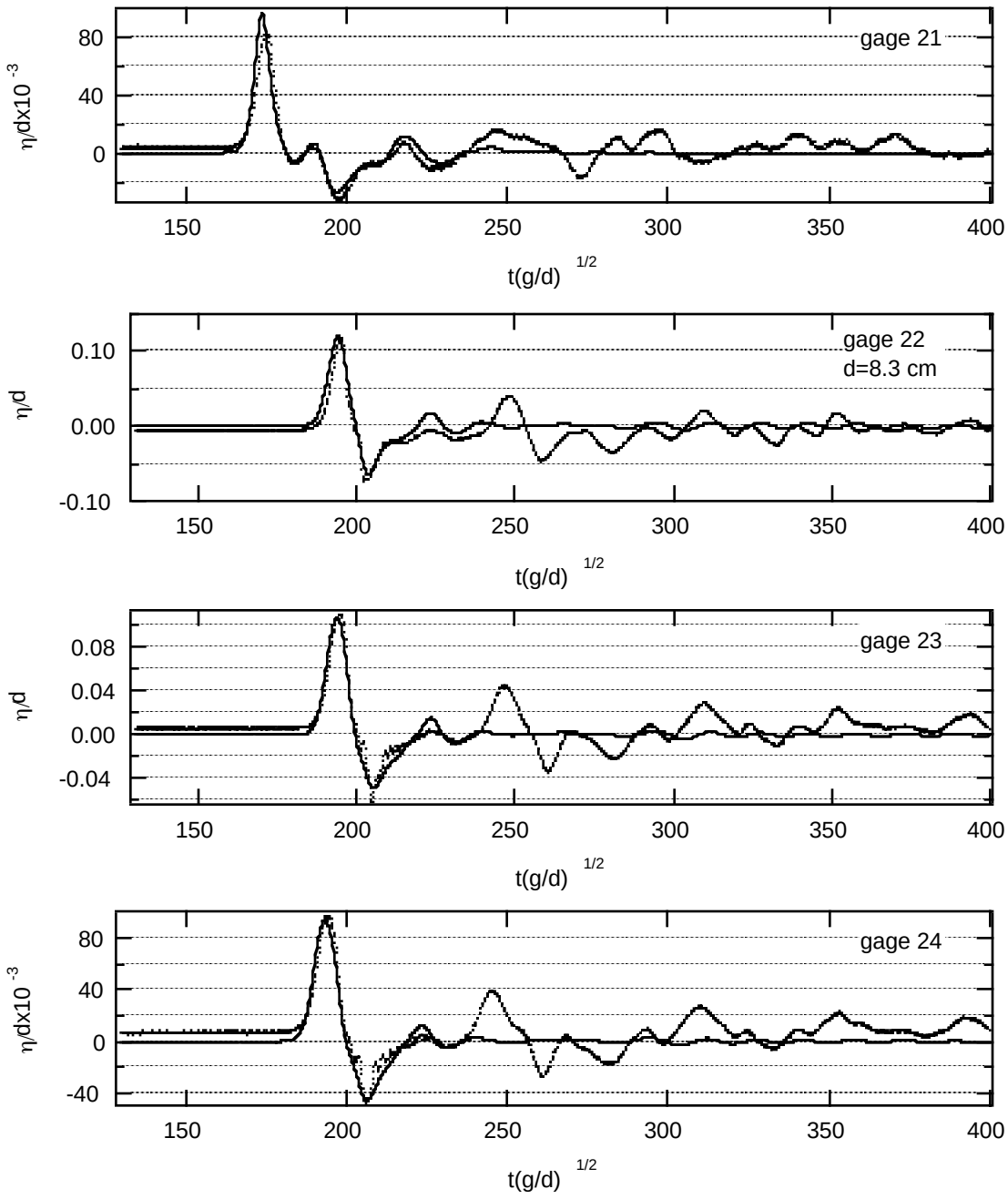

Figure 3.21 Comparison among the computed (solid lines) and laboratory records (dots) for the 0.1 wave.

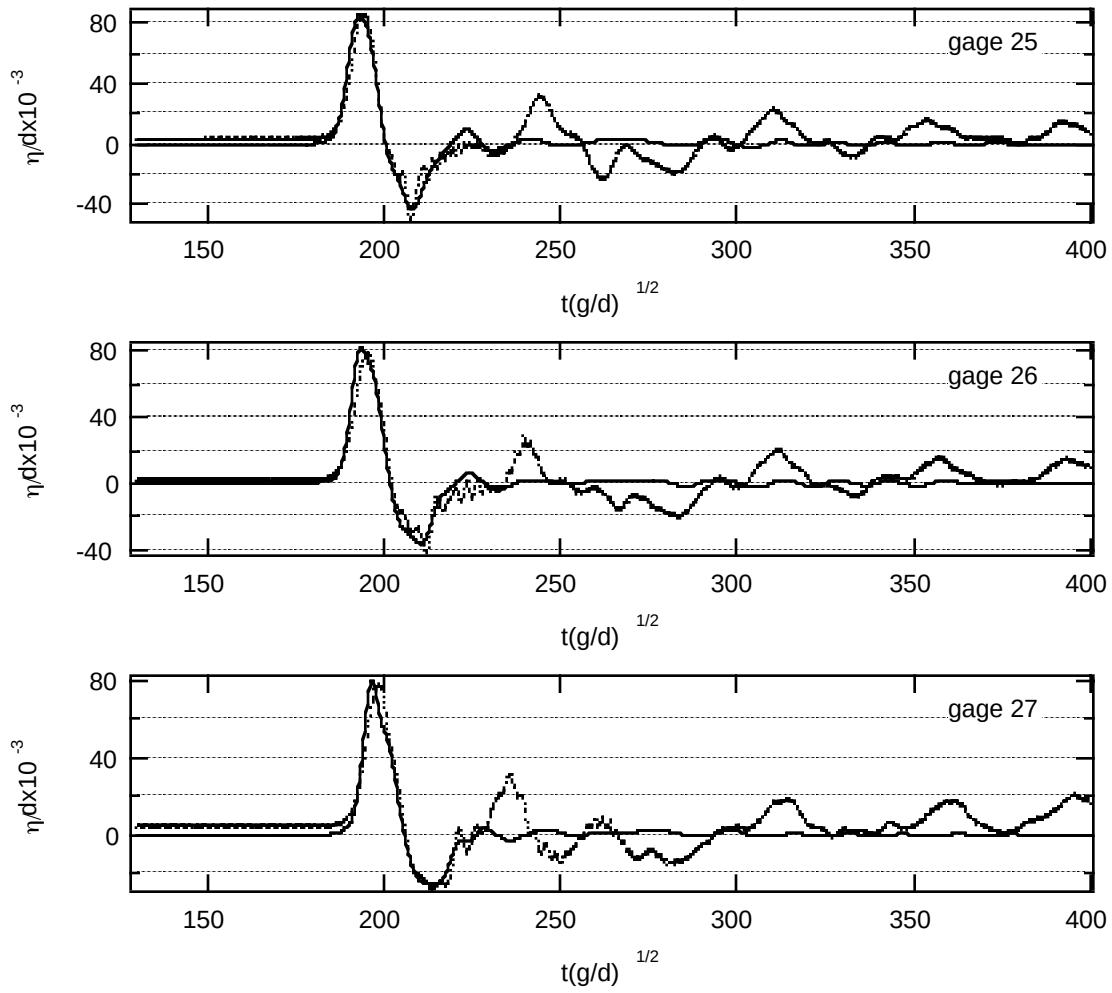

Figure 3.22 Comparison among the computed (solid lines) and laboratory records (dots) for the 0.1 wave.

The laboratory manifestation of the solitary waves with the initial amplitudes 0.1 break in only one location—on the back of the island where the trapped waves propagating from opposite sides collide with each other. The computed profiles on gages 22 - 27 show that wave breaking did not seriously affect the model predictions—the two profiles are still very close.

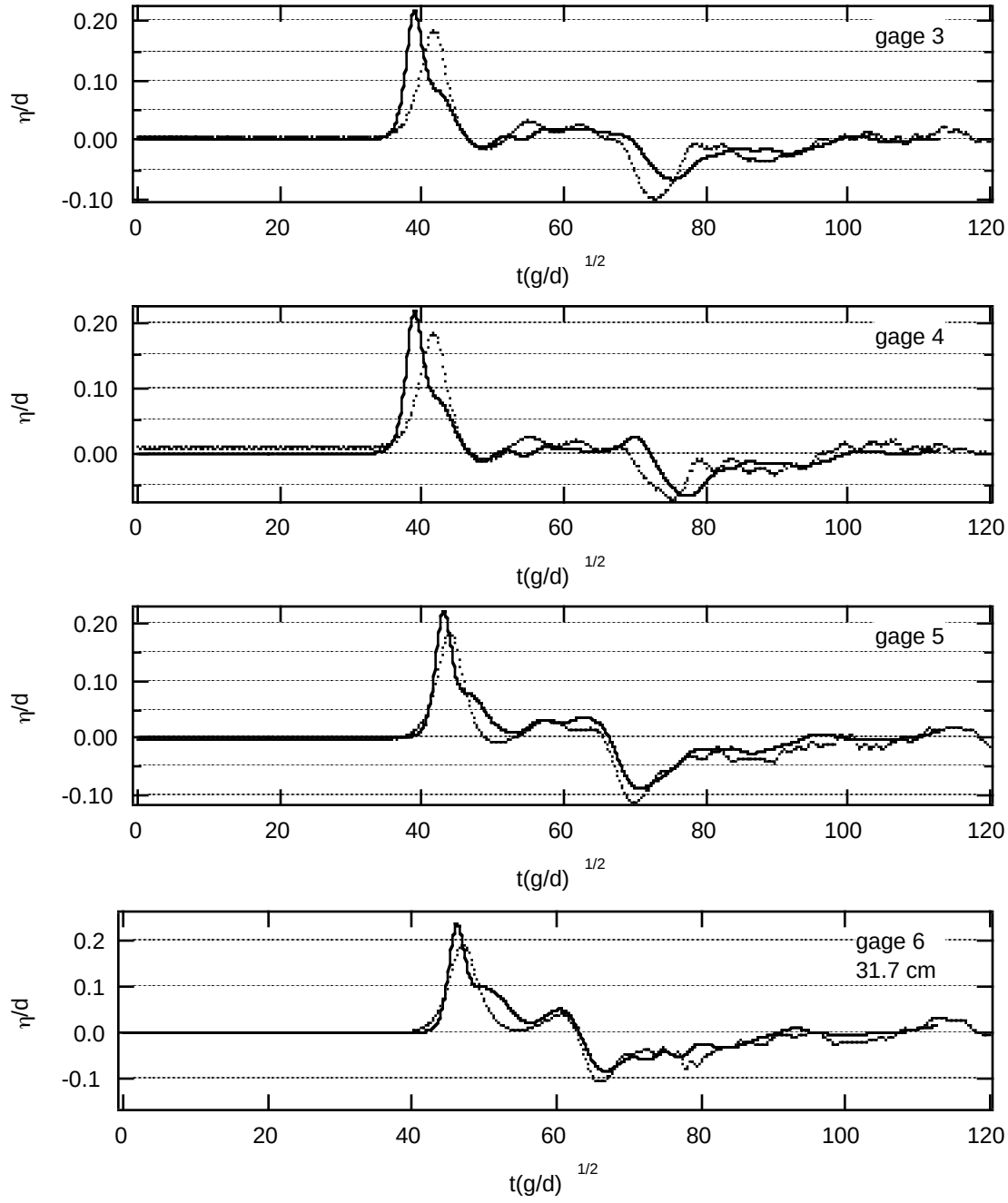

Figure 3.23 Comparison among the computed (sold lines) and laboratory (dots) records for the 0.2 wave.

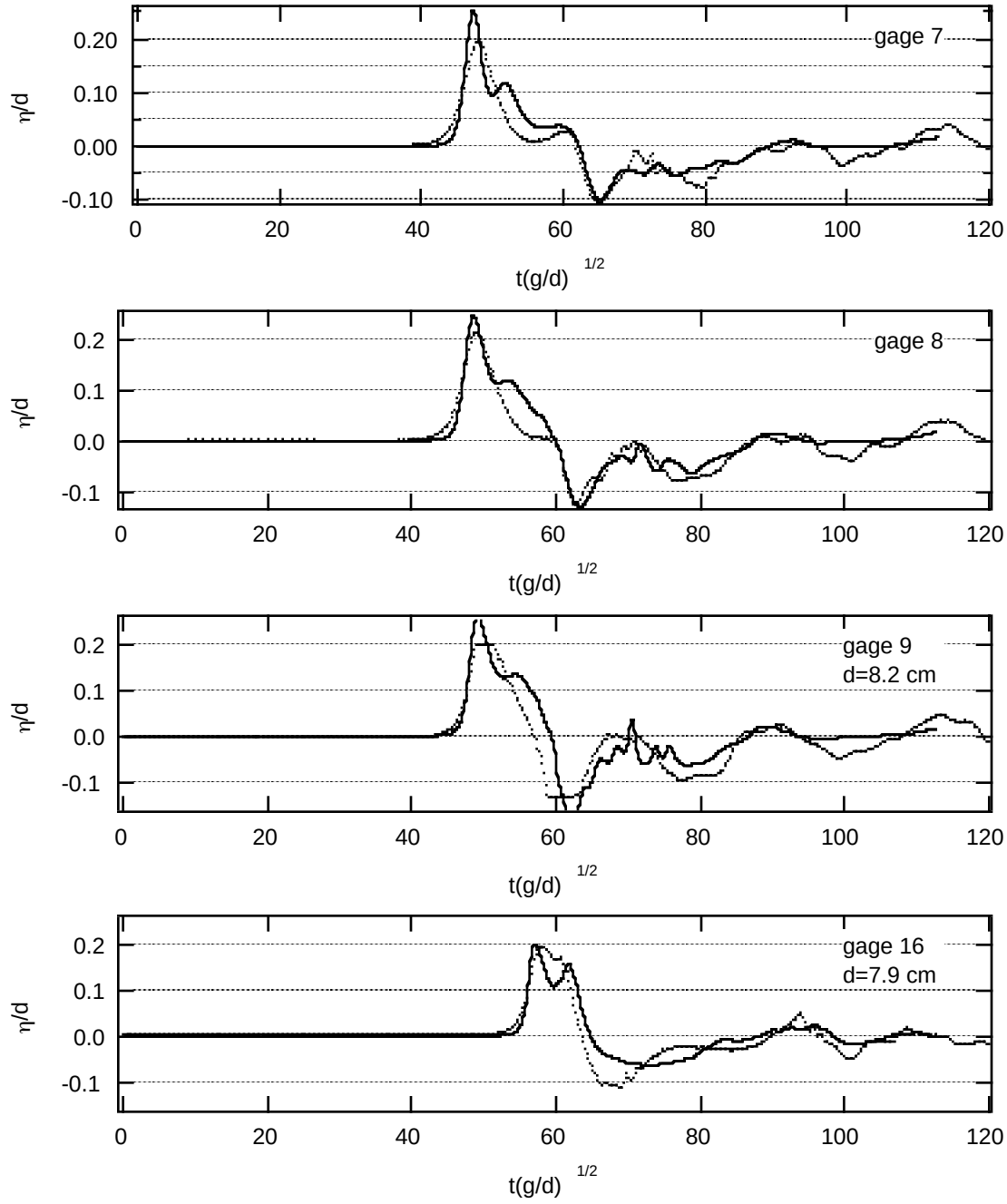

Figure 3.24 Comparison among the computed (sold lines) and laboratory (dots) records for the 0.2 wave.

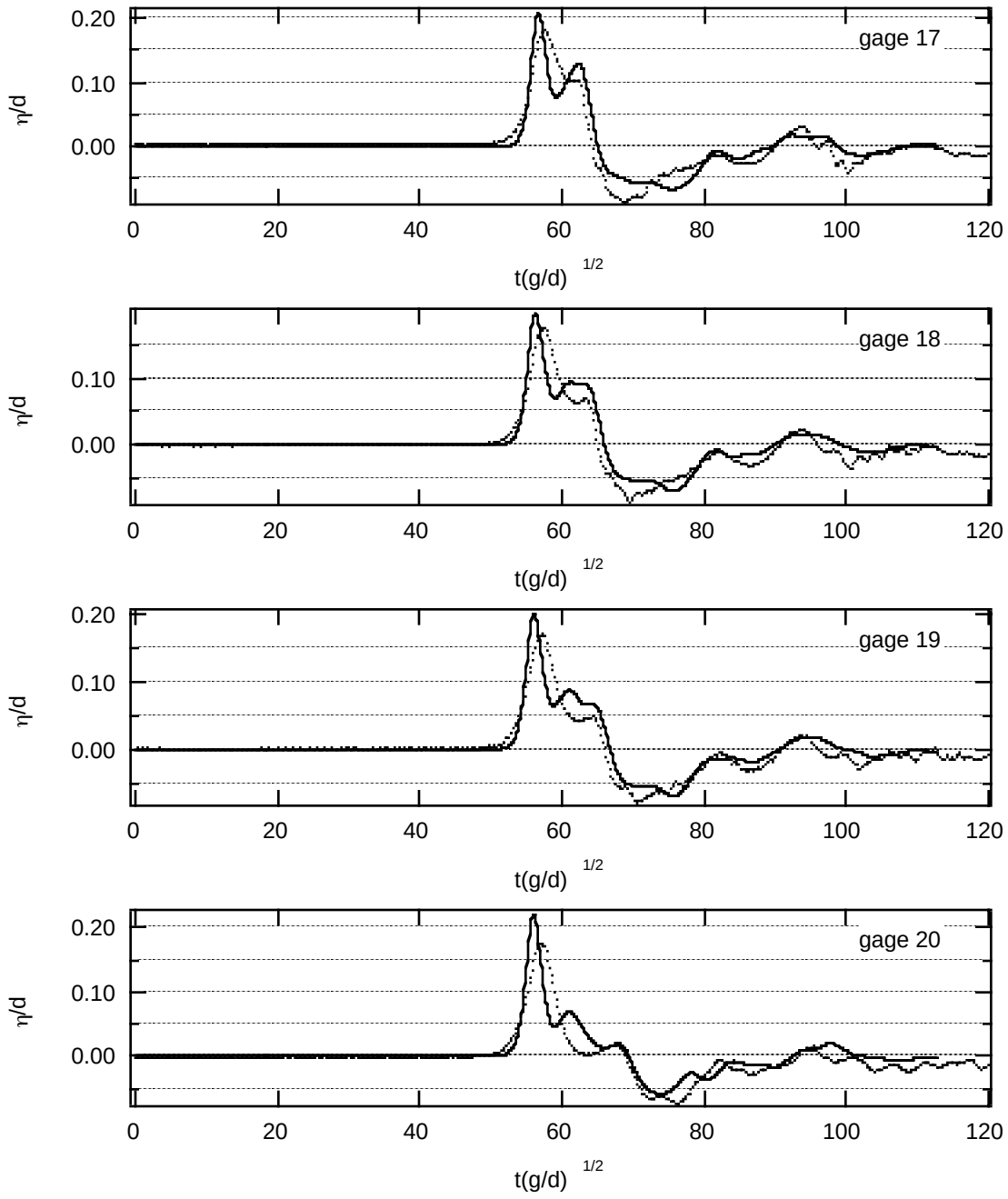

Figure 3.25 Comparison among the computed (sold lines) and laboratory (dots) records for the 0.2 wave.

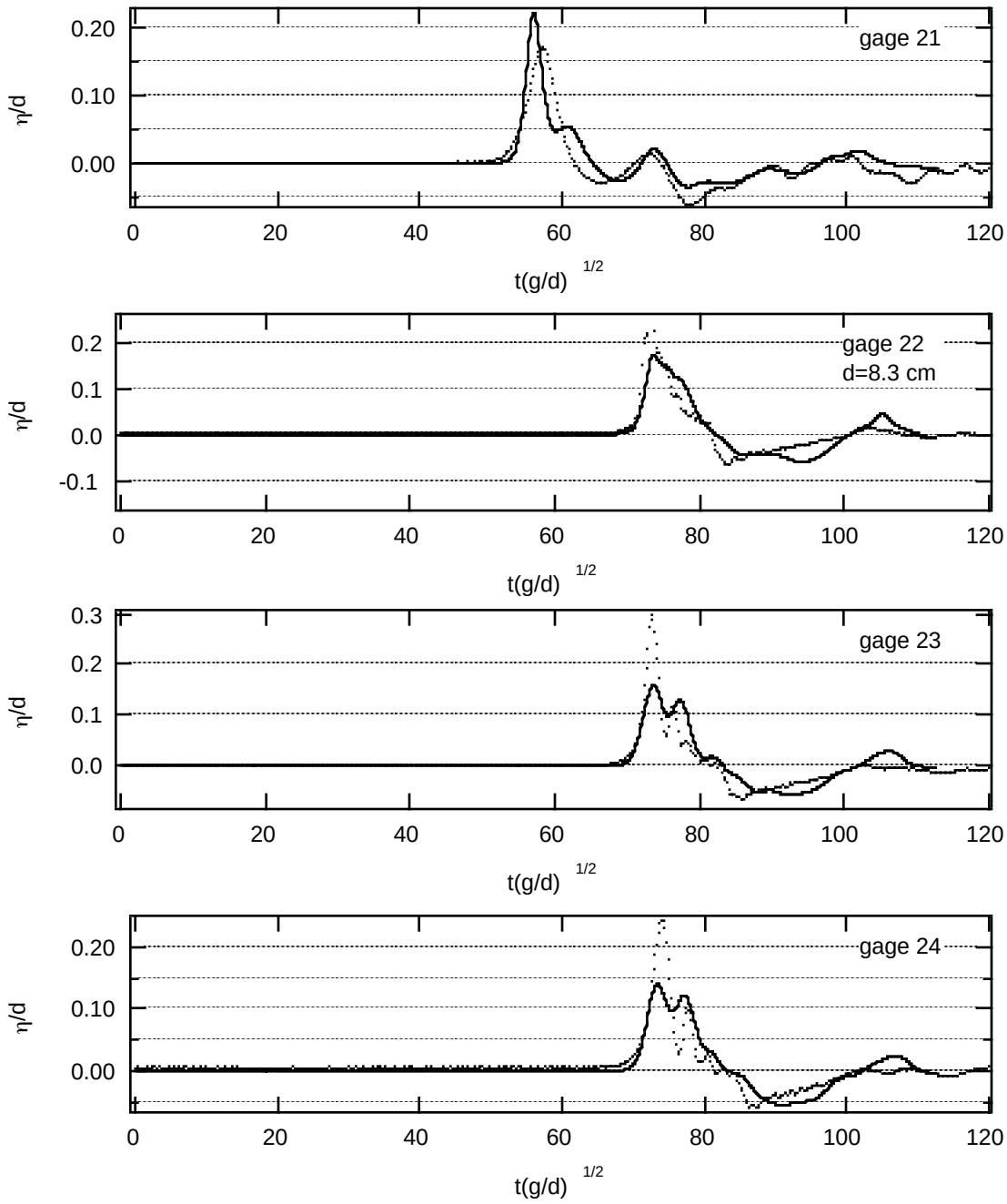

Figure 3.26 Comparison among the computed (sold lines) and laboratory (dots) records for the 0.2 wave.

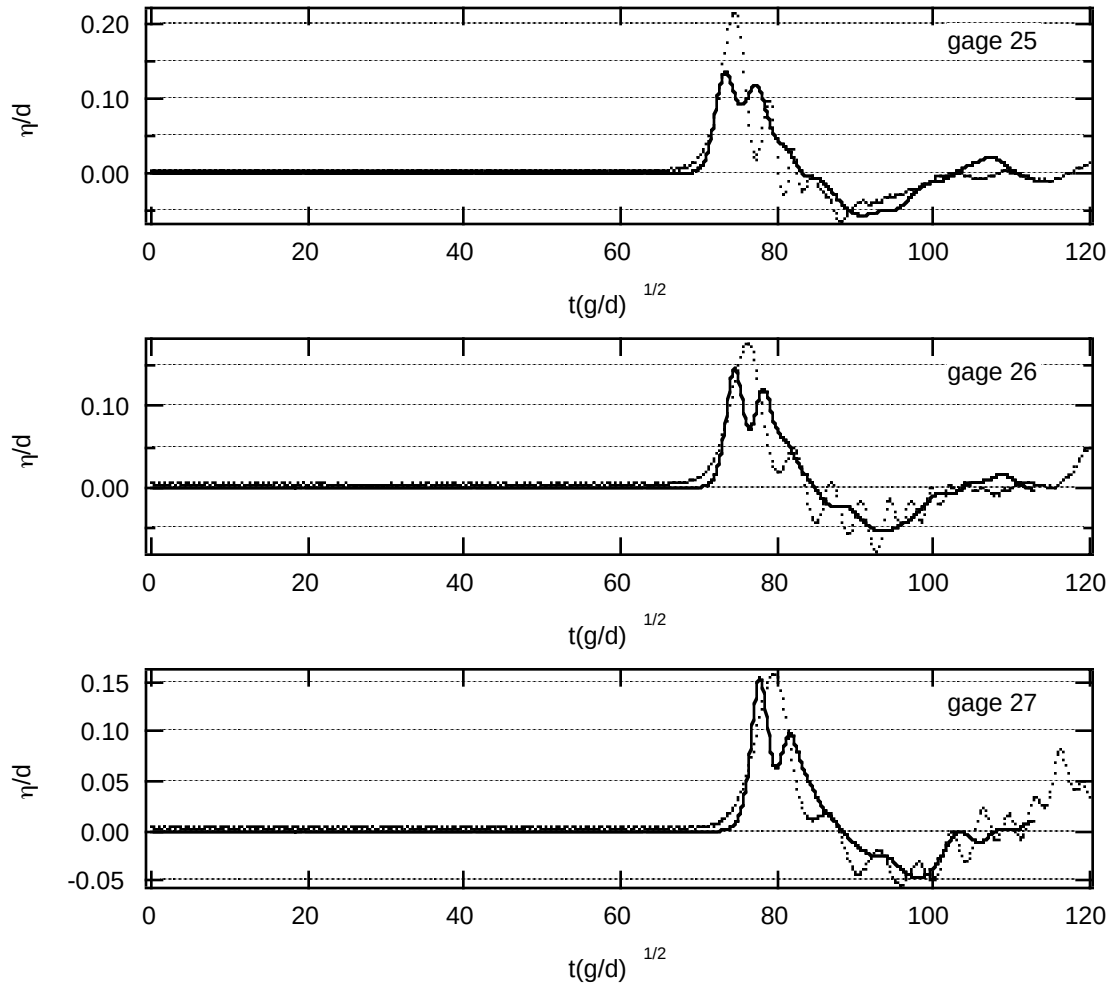

Figure 3.27 Comparison among the computed (sold lines) and laboratory (dots) records for the 0.2 wave.

The incident wave with $\eta/d = 0.2$ initial amplitude showed highly nonlinear behavior in the laboratory experiments. The wave broke over the slopes around the island. In shallow-water-wave theory breaking appears as a discontinuity of the solution of the nonlinear equations (3.23). Imposing conditions of mass and momentum conservation at the breaking discontinuity point, a generalized solution of the breaking wave is possible. The

SW solution of the breaking wave does not reproduce the details of the breaking front but, since the momentum and mass are conserved, it reflects the main features of the breaking wave profile.

Approximate numerical representations of generalized solutions of the shallow-water wave equations can be obtained either by imposing continuity conditions on the breaking front or by using dissipative nature of the particular numerical algorithm. The numerical model proposed here utilizes the latter method. It is dissipative "just enough" to avoid numerical instability and it carries the solution through breaking. The technique proved to be robust enough to model the runup process of the plunging plane wave climbing over 1:20 plane beach with an initial solitary wave height of $\eta/d = 0.3$ (Titov and Synolakis, 1995). Figure 3.23–Figure 3.27 show the comparison of the computed profiles with the laboratory measurements. The comparison suggests that the computed wave front steeps faster than the observed in the laboratory which is a well known effect of the long-wave theory and was observed also in the 1+1 computations of breaking waves by Titov and Synolakis (1995). The numerical model did not reproduce the height of splash off the lee side of the island, where the two breaking waves crash into each other (gage 23, see Figure 3.17). Modeling such effects should involve a higher-order wave theory since the SW theory does not take the vertical accelerations into account. Nevertheless, the maximum computed inland penetration is in a good agreement with the experiment data as shown below, suggesting that the horizontal velocities play the major role in the runup process.

Figure 3.28 and Figure 3.29 show the comparison among the computed and mea-

sured maximum runup values around the island for the incident waves with initial amplitudes η/d = 0.1 and 0.2, respectively. The figures suggest that the numerical model is able to compute the runup values adequately for these waves, in spite of breaking.

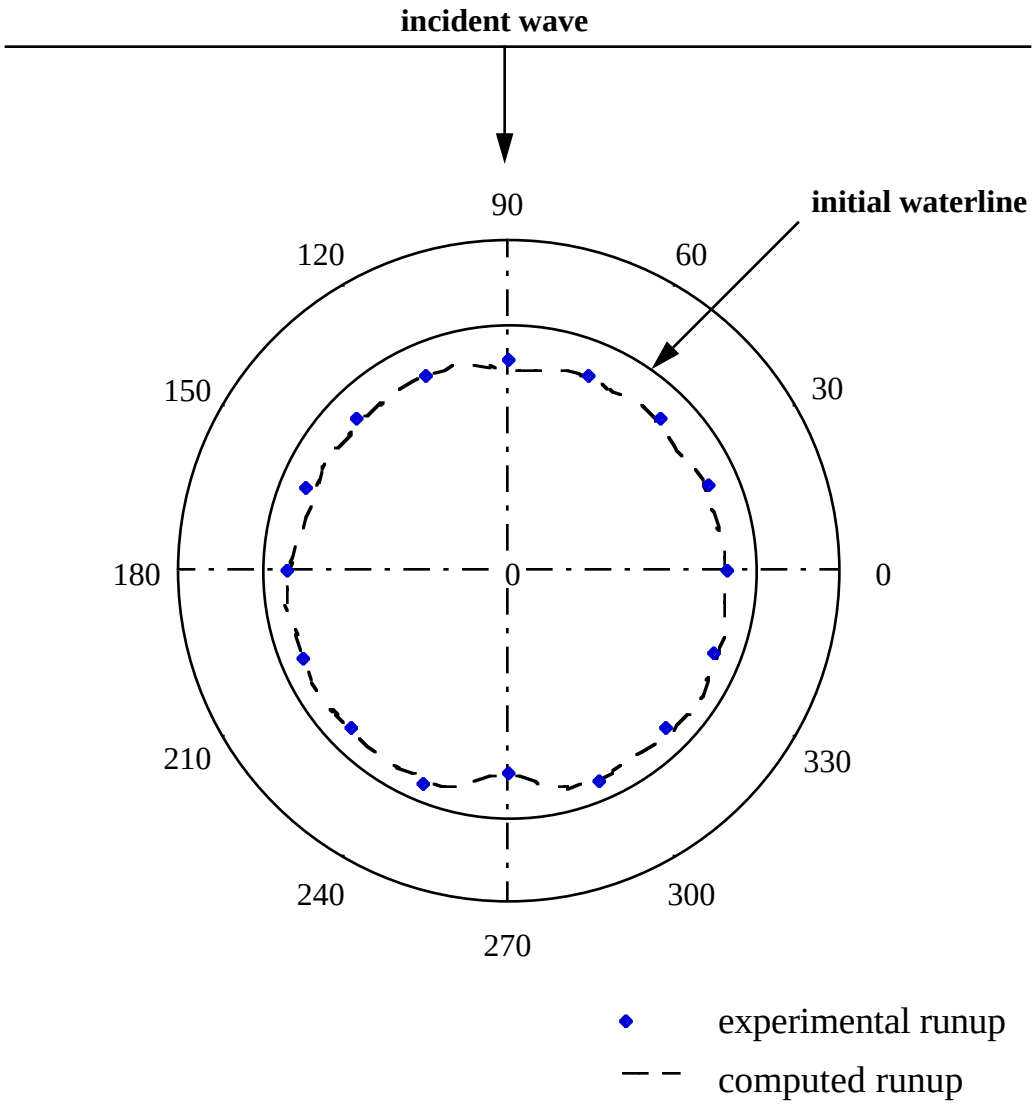

Figure 3.28 The comparison between computed and observed runup penetration on the conical island for 0.1 incident wave. The diagram shows a top view of the conical island with initial shoreline, measurement points of maximum runup and contours of the maximum computed wave penetration.

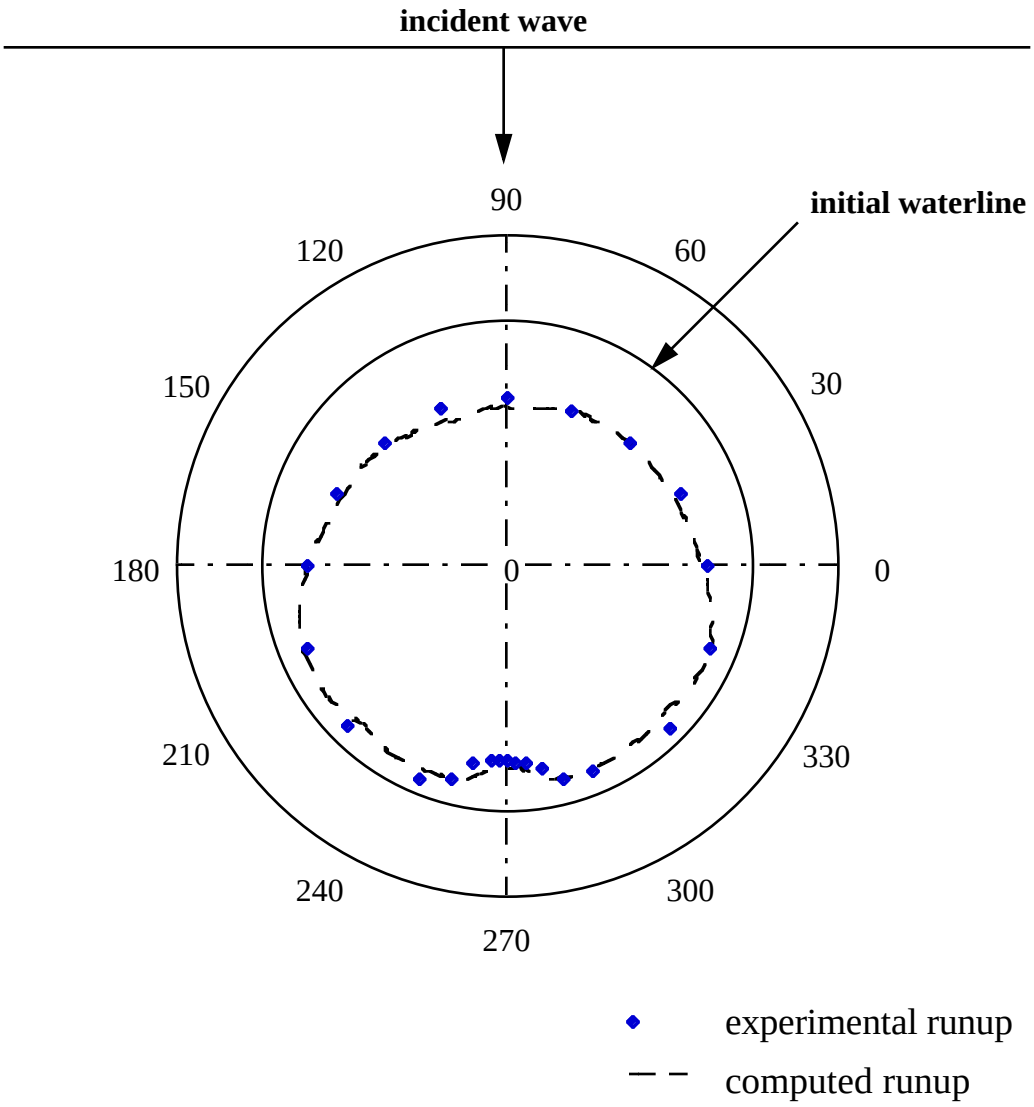

Figure 3.29 The comparison between computed and observed runup penetration on the conical island for 0.2 incident wave. The diagram shows a top view of the conical island with initial shoreline, measured points of maximum runup and contours of the maximum computed wave penetration.

3.4 Summary and conclusions

In this chapter a numerical model for the 3-D long waves propagation and runup on a beach with arbitrary topography was presented. The field model is the shallow-water wave equations, without friction factors or artificial viscosity. The 1+1 version of the model was previously tested with the maximum runup data of Hall and Watts (1953) and with the laboratory profile data and the analytical results of Synolakis (1987) and with Zelt's (1991) numerical results (Titov and Synolakis 1995). The Chapter describes a numerical method based on the splitting technique. The method allows for accurate implementation of the moving boundary conditions for the 3-D long wave runup problems. It is also computationally very efficient which permits simulations of large model problems. The method uses a variable space step in each direction and nested fine-resolution grids to resolve the changing scales of the wave dynamics during runup. We find that the model is able to reproduce main features of the wave runup process for wide range of initial wave parameters. The results suggest that at least for numerical schemes which are stable without additional dissipation, introduction of friction factors appears unnecessary. These comparisons with the laboratory data provide confidence for using the model for predicting the tsunami wave evolution of field events.